Magnetic states and Kondo screening in Weyl semimetals with chiral anomaly

Lin Li,[1,2] Jin-Hua Sun,[3] Zhen-Hua Wang,[2,4] Dong-Hui Xu,[5] Hong-Gang Luo,[4,6,*] and Wei-Qiang Chen[2,†]

[1]*College of Physics and Electronic Engineering, and Center for Computational Sciences, Sichuan Normal University, Chengdu, 610068, China*

[2]*Shenzhen Institute for Quantum Science and Engineering and Department of Physics, Southern University of Science and Technology, Shenzhen 518055, China*

[3]*Department of Physics, Ningbo University, Ningbo 315211, China*

[4]*Beijing Computational Science Research Center, Beijing 100084, China*

[5]*Department of Physics, Hubei University, Wuhan 430062, China*

[6]*Center of Interdisciplinary Studies and Key Laboratory for Magnetism and Magnetic Materials of the Ministry of Education, Lanzhou University, Lanzhou 730000, China*

(Received 15 March 2018; revised manuscript received 13 July 2018; published 7 August 2018)

We theoretically study the localized magnetic states and the Kondo screening of a magnetic impurity in the bulk of Weyl semimetals (SMs). The linear dispersion near the Weyl nodes and the anomalous broadening of the impurity level lead to a nonvanishing magnetic moment in a wide region of parameters. The magnetic susceptibility is significantly enhanced by increasing the chirality imbalance for the chemical potential fixed at the Weyl nodes. The Kondo effect takes place whenever the chemical potential is tuned away from the nodes. The low-temperature susceptibility is determined by both the Kondo screening and the broadening of the magnetic impurity level. In the presence of chiral anomaly, the Kondo screening displays opposite behaviors for the chemical potential situated below and above the Weyl nodes. The magnetic susceptibility can be tuned by the charge imbalance of the nodes, which provides a scheme to study the chiral anomaly in Weyl SMs.

DOI: 10.1103/PhysRevB.98.075110

I. INTRODUCTION

The discovery of the three-dimensional (3D) topological materials has attracted extensive attention in the last decade [1–5]. For example, the topological insulators characterized by metallic spin-polarized surface states connecting the bulk valence and conduction bands, have great potentials in spintronics [6–8]. More recently the three-dimensional Dirac SMs with topologically nontrivial bulk states are experimentally observed in Na_3Bi [9] and Cd_3As_2 [10–12]. The Dirac SMs are 3D counterparts of graphene that the conduction and valence energy bands with linear dispersions touch at Dirac nodes [13]. Breaking either time-reversal symmetry or inversion symmetry splits a Driac node into a pair of Weyl nodes with opposite chirality [14]. Topological Weyl states have been observed in TaAs [15–17] and NbAs [18], which possess interesting physics, such as the chiral anomaly generated large negative magnetoresistance under the parallel magnetic and electric fields [19,20]. This chiral magnetic effect (CME) is a solid evidence for the charge imbalance between the Weyl nodes [21–25]. Recently, other schemes are theoretically proposed to detect the chiral anomaly, such as the nonlocal transport [26], optical conductivity [27–30], and the plasmon modes in Weyl SMs [31].

The Kondo effect originating from the screening of a magnetic impurity by the itinerant conduction electrons has been well understood in the community of condensed matter physics [32,33]. At the temperature $T < T_K$, the formation of localized Kondo singlet state reflects the characteristics of conduction band structures [34–39], where T_K is the Kondo temperature. Therefore, one may suppose that the chirality imbalance near the Weyl nodes can be investigated through the Kondo effect. For a magnetic impurity in the bulk of Dirac and Weyl SMs, the Kondo screening depends on the chemical potential due to the particular band structure near the nodes. When the chemical potential is tuned near the Weyl nodes, the Kondo screening is very weak due to the lower density of states [40]. The variation of Kondo temperature with the chemical potential is determined by the symmetry breaking of the hosts [41]. In the presence of long-range scalar disorder, the Kondo effect is characterized by a distribution of Kondo temperature, which generates a strong non-Fermi-liquid behavior around the nodes [42]. Recently, the Kondo screening of a magnetic impurity by the tilted Dirac surface states and the Weyl SMs Fermi arcs has been investigated by a variational method [43,44]. The spin correlation function between the magnetic impurity and Dirac surface states shows power-law decay with respect to the spatial displacements, and displays strongly spatial anisotropy due to the spin-orbit coupling [43,45]. The spatial spin-spin correlations in Fermi arcs exhibit high spatial anisotropy, which can be tuned by chemical potential [44].

In the present work we focus on the impacts of chiral anomaly on the localized magnetic states of a magnetic impurity and its Kondo screening in Weyl SMs. As shown schematically in Fig. 1, the magnetic impurity is coupled with the Weyl nodes with chirality dependent chemical potentials

*luohg@lzu.edu.cn
†chen.wq@sustc.edu.cn

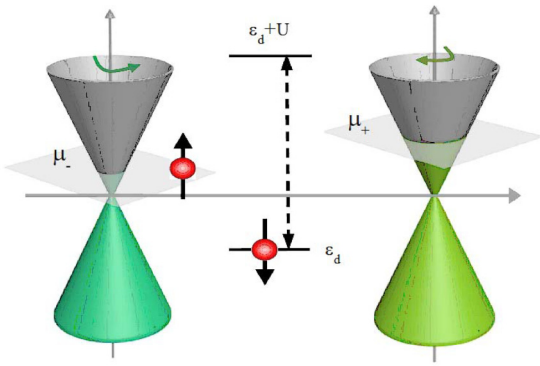

FIG. 1. The Kondo screening of a magnetic impurity in the bulk of Weyl SMs, where a spin-down (-up) electron on the impurity level ε_d is replaced by a spin-up (-down) electron through the empty or double occupation virtual states. The chiral anomaly introduces the charge imbalance between the Weyl nodes with opposite chirality ($h = \pm$), and the chemical potentials $\mu_\pm = \mu_0 \pm \delta\mu/2$. μ_0 is the chemical potential in the absence of chiral anomaly, and $\delta\mu$ denotes the charge imbalance.

$\mu_\pm = \mu_0 \pm \delta\mu/2$, where the chirality imbalance $\delta\mu$ can be introduced and tuned by parallel magnetic and electric fields [21,29,31]. In such a system, the phase boundary between the magnetic and nonmagnetic regions shows particle-hole asymmetry due to the linear dispersion near the Weyl nodes. The anomalous broadening of the magnetic impurity level leads to the local moment existing in a wide region of parameters, even extending to some empty or double occupied regions. In the presence of chiral anomaly, the range of magnetic state is reduced in conventional single occupied regions, while the range of magnetic moment is enlarged in double occupied and empty regions. These characteristics in the formation of localized magnetic moment suggest that some interesting features would be observed in the Kondo screening of the local moment. It is found that the Kondo effect is absent for the chemical potential lies at the nodes ($\mu_0 = 0$). By increasing the coupling or the chirality imbalance, the susceptibility is significantly enhanced due to the anomalous broadening of the impurity level. The Kondo screening takes place whenever $\mu_0 \neq 0$, and the susceptibility is determined by both the Kondo screening and the broadening of the magnetic impurity level. In the presence of chiral anomaly, the Kondo screening is suppressed when the chemical potential is tuned above the Weyl nodes $\mu_0 > 0$. On the contrary, the Kondo screening is significantly enhanced by the chirality imbalance for $\mu_0 < 0$. The magnetic susceptibility can be conveniently controlled by the chirality imbalance. Thus, the chiral anomaly in Weyl SMs can be detected by measuring the low-temperature susceptibility.

The paper is organized as follows. In Sec. II we present the model of a magnetic impurity coupled with the Weyl nodes with opposite chirality. In Sec. III we discuss the localized magnetic states of a magnetic impurity in Weyl SMs. In Sec. IV the Kondo screening of the local moment and the behaviors of magnetic susceptibility are discussed in the presence of chiral anomaly. The influence of the time-reversal symmetry breaking and the Zeeman splitting induced internode spin-flipping scattering (SFS) processes are also discussed. A brief conclusion is devoted to Sec. V.

II. HAMILTONIAN

The Hamiltonian of a magnetic impurity in Weyl SMs can be read

$$H = H_0 + H_V + H_d, \tag{1}$$

where

$$H_0 = \sum_{\mathbf{k}} \Psi^\dagger_{\mathbf{k}}[\tau^z(\upsilon_F \mathbf{k} - \mathbf{Q}) \cdot \sigma - \mu]\Psi_{\mathbf{k}} \tag{2}$$

describes the bulk electrons near the Weyl nodes $\mathbf{Q} = (0, 0, \pm Q_z)$, and the vector $\mathbf{k} = (k_x, k_y, k_z)$. σ and τ are the Pauli matrices acting on spin and chirality space, respectively. The basis vector reads $\Psi_{\mathbf{k}} = (c_{+\mathbf{k}\uparrow} \quad c_{+\mathbf{k}\downarrow} \quad c_{-\mathbf{k}\uparrow} \quad c_{-\mathbf{k}\downarrow})^T$, where the operators $c^\dagger_{h\mathbf{k}s}$ ($c_{h\mathbf{k}s}$) stands for the creation (annihilation) of a conduction electron in the Weyl nodes with opposite chirality $h = \pm$, and $s(=\uparrow, \downarrow)$ is the spin index, υ_F denotes the Fermi velocity. The notation $\mu = \mathrm{diag}(\mu_+, \mu_+, \mu_-, \mu_-)$ represents the chemical potentials of the nodes. The impurity is described by

$$H_d = \sum_{\mathbf{s}} \varepsilon_{ds} d^\dagger_s d_s + U n_{ds} n_{d\bar{s}}, \tag{3}$$

where ε_{ds} is impurity level, U represents the Coulomb repulsion, $d^\dagger_s(d_s)$ denotes the creation (annihilation) operator of d electrons, and $n_{ds} = d^\dagger_s d_s$. In Weyl SMs, the spin degeneracy of impurity level would be removed due to the time-reversal symmetry breaking. Then, one can denote $\varepsilon_{ds} = \varepsilon_d + s_z E_Z$ with $s_z = \pm 1/2$, and E_Z is the Zeeman interaction of the impurity level. In general, the electric field plays a role to shift the level ε_d slightly.

The hybridization between the conduction electrons and the magnetic impurity is

$$H_V = \sum_{h\mathbf{k}s} (V_{\mathbf{k}} c^\dagger_{h\mathbf{k}s} d_s + \mathrm{H.c.}). \tag{4}$$

By diagonalizing the noninteracting Hamiltonian H_0, we obtain the single-particle energy $\varepsilon_{1hk(2hk)} = -\mu_h \pm \upsilon_F \lambda_{hk}$ with $\lambda_{hk} = h\sqrt{(k_z - hQ_z)^2 + k_x^2 + k_y^2}$. The corresponding four eigenstates are $\alpha^\dagger_{1h\mathbf{k}(2h\mathbf{k})} = c^\dagger_{h\mathbf{k}\downarrow} + \eta_{1hk(2hk)} c^\dagger_{h\mathbf{k}\uparrow}$ with $\eta_{1hk(2hk)} = \frac{k_z \pm |\lambda_{hk}|}{k_+}$ and $k_+ = k_x + ik_y$. Then the noninteracting Hamiltonian can be written as

$$H_0 = \sum_{ih\mathbf{k}} \varepsilon_{ihk} \alpha^\dagger_{ih\mathbf{k}} \alpha_{ih\mathbf{k}}, \tag{5}$$

and the hybridization term becomes

$$H_V = \sum_{ih\mathbf{k}} (-1)^{i-1} V_0 (\xi_{hk} \alpha^\dagger_{ih\mathbf{k}} d_\uparrow - \zeta_{hk} \alpha^\dagger_{ih\mathbf{k}} d_\downarrow), \tag{6}$$

where $i = 1, 2$, $\xi_{hk} = \frac{k_+}{2\lambda_{hk}}$, $\zeta_{hk} = \frac{k_z + |\lambda_{hk}|}{2\lambda_{hk}}$, and the coupling amplitude is taken $V_k = V_0$ for simplification. In Wely SMs, the spin-orbit coupling couples the spin and orbital degrees of freedom, then creates an indirect coupling between the impurity and the conduction electrons with opposite spin as shown Eq. (6).

III. LOCALIZED MAGNETIC STATES

One of the conspicuous characteristics of Weyl SMs is the linear dispersion along three-momentum directions near the Weyl nodes. It is found that a magnetic impurity would introduce interesting physics due to the linear dispersion of conduction electrons, such as the anomalous localized magnetic states [46–48] and the pseudogap Kondo effect in graphene [49–52]. In this section we discuss the formation of magnetic moment for an impurity coupled with the bulk states of Weyl SMs. The localized magnetic states can be studied in the frame of Hartree-Fock approximation (HFA) [46,53]. The Hamiltonian Eq. (1) can be treated by the equation of motion approach (EOM) [54]

$$\omega\langle\langle A;B\rangle\rangle = \langle[A,B]_+\rangle + \langle\langle[A,H]_-;B\rangle\rangle, \tag{7}$$

where the subscript $\pm$ stands for the anticommutation (commutation) relationship, and $\langle\langle A;B\rangle\rangle$ denotes the retarded Green's function (GF) composed by the operators A and B. The impurity GF can thus be written as

$$\omega\langle\langle d_s;d_s^\dagger\rangle\rangle = 1+\varepsilon_{ds}\langle\langle d_s;d_s^\dagger\rangle\rangle + U\langle\langle d_s n_{d\bar{s}};d_s^\dagger\rangle\rangle + \sum_{ih\mathbf{k}} V_{ihks}^*\langle\langle \alpha_{ih\mathbf{k}};d_s^\dagger\rangle\rangle, \tag{8}$$

with $V_{ihk\uparrow} = -V_0(-1)^i\xi_{hk}$ and $V_{ihk\downarrow} = V_0(-1)^i\zeta_{hk}$. The HFA can be reached by taking the approximation $\langle\langle d_s n_{d\bar{s}};d_s^\dagger\rangle\rangle \approx \langle n_{d\bar{s}}\rangle\langle\langle d_s;d_s^\dagger\rangle\rangle$, then we obtain

$$\langle\langle d_s;d_s^\dagger\rangle\rangle = \frac{1}{\omega-\varepsilon_{ds}-\Xi_s^0(\omega)\eta_s(\omega)-U\langle n_{d\bar{s}}\rangle}, \tag{9}$$

where the notations are $\Xi_s^0(\omega) = \Gamma_0\Theta_F\sum_h[(-i\pi - \frac{2D}{\omega+\mu_h} + \ln\frac{|D-\omega-\mu_h|}{|-D-\omega-\mu_h|})(\omega+\mu_h)^2]$, $\eta_s(\omega) = 1+\frac{\Xi_s^0(\omega)}{\omega-\varepsilon_{d\bar{s}}-\Xi_s^0(\omega)-U\langle n_{d\bar{s}}\rangle}$, $\Gamma_0 = \pi|V_0|^2/D$, and $\Theta_F = D/2\pi^2\upsilon_F^3$. In the present work, the half-band width $D=1$ is taken as the unit of energy. The occupation is $\langle n_{ds}\rangle = -\frac{1}{\pi}\int f(\omega)\mathrm{Im}\langle\langle d_s;d_s^\dagger\rangle\rangle d\omega$, and the Fermi distribution function is defined in a pseudoequilibrium form $f(\omega) = \sum_h[f_h(\omega)(\omega+\mu_h)^2]/\sum_h(\omega+\mu_h)^2$ [55,56], $f_h(\omega)$ is the Fermi function of the conduction electrons on the Weyl nodes. Then, the GF and the occupation on impurity level can be numerically obtained by self-consistently calculations. By tuning the parameters, such as μ_0, ε_d, and Γ_0, one can always obtain a nonmagnetic solution ($n_{d\uparrow} = n_{d\downarrow}$) based on the GF given by Eq. (9), while the magnetic solutions ($n_{d\uparrow} \neq n_{d\downarrow}$) are merely obtained in the magnetic regions [53]. The localized states are mainly determined by exchange coupling between the magnetic impurity and the conduction bands. The Zeeman splitting is believed to have no qualitative influence on the local moment of the magnetic impurity, and we take $E_Z = 0$ in the calculations for simplification.

In Fig. 2 we show the localized magnetic state region as a function of $(\mu_0-\varepsilon_d)/U$ and $\pi\Gamma_0/U$ in the absence of chirality imbalance ($\delta\mu = 0$). Differing from that for a magnetic impurity in normal metal [53], the phase boundary between the magnetic and nonmagnetic state is not symmetric with respect to $(\mu_0-\varepsilon_d)/U = 0.5$. In the case of $\mu_0 > 0$, the magnetic impurity possesses local moment even when the impurity level is above the Fermi level ($\mu_0-\varepsilon_d < 0$), as shown in Fig. 2(a). The magnetic regions, corresponding

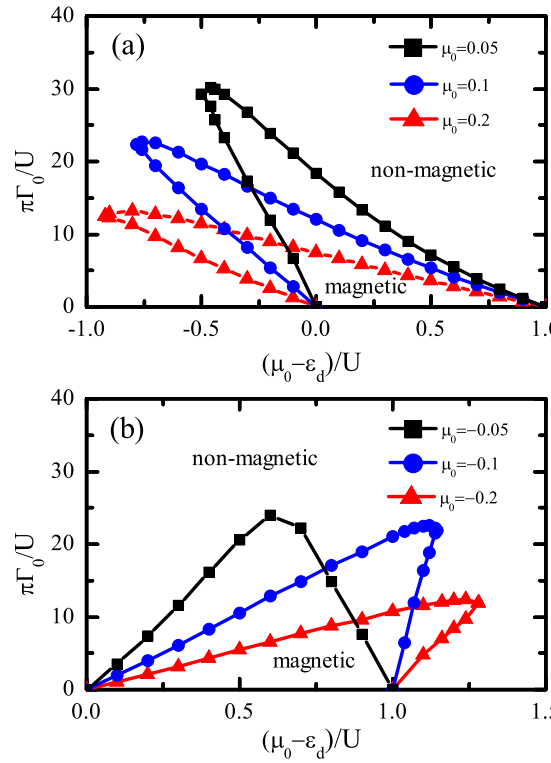

FIG. 2. The phase boundary between the magnetic and nonmagnetic regions of a magnetic impurity coupled with two Weyl nodes. The chemical potential μ_0 is tuned above (a) and below (b) the nodes with $\mu_0 = \pm0.05, \pm0.1, \pm0.2$, and other parameters are $E_z = 0$, $Q_z = 0.1$, $U = 2$, and the temperature $T = 0$.

to the chemical potentials $\mu_0(= 0.05, 0.1, 0.2)$, are attributed to anomalous broadening of impurity level around the Fermi level. As shown in the inset of Fig. 4(a), the impurity level gets close to the Weyl nodes ($\mu_0 = 0$) by increasing the coupling Γ_0, and the half-width of the level becomes narrower due to the vanishing of DOS. In fact, the formation of local moment in empty-occupied regions ($\mu_0-\varepsilon_d < 0$) has been obtained for a magnetic adatom on graphene [46]. In that case, the linear dispersion around the Dirac point leads to the anomalous broadening of impurity level near the Fermi level for $\varepsilon_d > \mu_0$. Oppositely, in the case of $\mu_0 < 0$, the magnetic moment exists even when the impurity is in double occupied states [$(\mu_0-\varepsilon_d)/U > 0$], see the magnetic regions with $\mu_0 = -0.1, -0.2$. The phase boundary between magnetic and nonmagnetic regions shows particle-hole asymmetry for the chemical potential μ_0 posited above and below the Weyl nodes. In the presence of chiral anomaly, the chemical potential differences $\delta\mu$ are introduced near the Weyl nodes. Correspondingly, the localized magnetic states are influenced by the chiral anomaly. In Figs. 3(a) and 3(b) we show the range of the magnetic states is reduced by the chirality imbalance $\delta\mu$ in a conventional single occupied region $0 < (\mu_0-\varepsilon_d)/U < 1$. However, the range of the magnetic states are enlarged in the empty regions $(\mu_0-\varepsilon_d)/U < 0$ as shown Fig. 3(a), where the magnetic impurity situates above the Fermi level. Oppositely, the magnetic regions are expanded in double occupied state when the chemical potential is tuned below the Weyl nodes, see Fig. 3(b). In addition, the magnetic states extends to

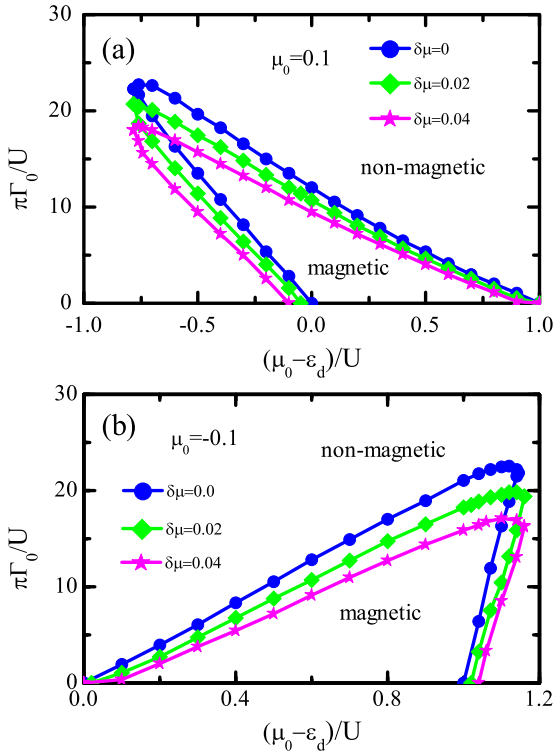

FIG. 3. The influence of the chiral anomaly on the phase boundary between the magnetic and nonmagnetic states of a magnetic impurity in Weyl SMs. (a) and (b) The chemical potential situates above and below the Weyl nodes with $\mu_0 = \pm 0.1$ and $\delta\mu = 0.0, 0.02, 0.04$. Other parameters are the same with that in Fig. 2.

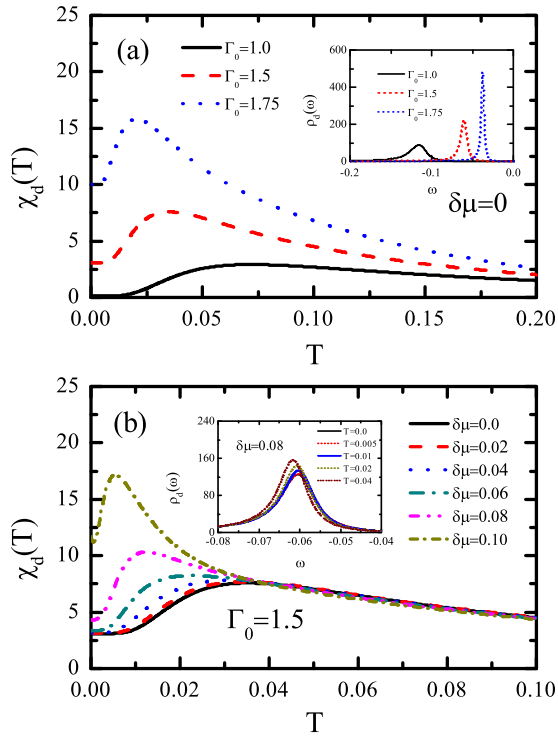

FIG. 4. The susceptibility of a magnetic impurity in Weyl SMs with the chemical potential $\mu_0 = 0$. (a) The enhancement of magnetic susceptibility by increasing the coupling amplitudes $\Gamma_0 = 1.0, 1.5, 1.75$ in the absence of chirality imbalance $\delta\mu = 0$. The inset is the local density of states (LDOS) of the magnetic impurity. (b) The variation of magnetic susceptibility in the presence of chiral anomaly with $\mu_\pm = \pm\delta\mu/2$, and the coupling amplitude $\Gamma_0 = 1.5$. The inset is the temperature dependent LDOS for the chiral imbalance $\delta\mu = 0.08$. Other parameters are the impurity level $\varepsilon_d = -0.3$, $Q_z = 0.1$, and the Coulomb repulsion $U = 2.0$.

$(\mu_0 - \varepsilon_d)/U < 0 (> 1)$ for $\mu_0 = \pm 0.1$ around the atomic limit ($\Gamma_0 \to 0$). This is attributed to the chirality imbalance near the Weyl nodes. These characteristics of the localized magnetic states in Weyl SMs inspire us to study the Kondo screening of the local moment [41,49,57].

IV. KONDO EFFECT IN WEYL SMS WITH CHIRAL ANOMALY

To capture the Kondo effect one must take some approximations beyond the frame of HFA. In the present work we treat the higher-order GF $\langle\langle d_s n_{d\bar{s}}; d_s^\dagger\rangle\rangle$ in Eq. (8) by using the Lacroix's approximation scheme, see the Appendix, which can qualitatively describe the Kondo physics at low temperature [58,59]. After some straightforward calculations, the GF can be obtained as

$$\langle\langle d_s; d_s^\dagger\rangle\rangle = \frac{1+U\frac{\langle n_{d\bar{s}}\rangle+Q_s(\omega)}{\omega-\varepsilon_{ds}-U-\Xi_s(\omega)}}{\omega-\varepsilon_{ds}-\Xi_s^0(\omega)\eta_s(\omega)+U\frac{\Omega_s(\omega)+Q_s(\omega)\Xi_s^0(\omega)\eta_s(\omega)}{\omega-\varepsilon_{ds}-U-\Xi_s(\omega)}}, \tag{10}$$

with $\Xi_s(\omega) = \Xi_s^0(\omega) + \Xi_s^1(\omega) + \Xi_s^2(\omega)$, $\Xi_s^l(\omega) = \frac{\Gamma_0}{\pi}\sum_{ihk}\frac{\zeta_{hk}^2+\xi_{hk}^2}{\omega-\varepsilon_{lihks}}$, $l = (1, 2)$, $\varepsilon_{1ihks} = -\varepsilon_{ihk} + \varepsilon_{d\bar{s}} + \varepsilon_{ds} + U$, and $\varepsilon_{2ihks} = \varepsilon_{ihk} - \varepsilon_{d\bar{s}} + \varepsilon_{ds}$. Other notations are $\Omega_s(\omega) = A_{1s}(\omega) + A_{2s}(\omega)$ and $Q_s(\omega) = B_{1s}(\omega) - B_{2s}(\omega)$, with

$$A_{ls}(\omega) = \frac{\Gamma_0}{\pi}\sum_{ihk}\frac{\left(\zeta_{hk}^2+\xi_{hk}^2\right)f(\varepsilon_{ihk})}{\omega-\varepsilon_{lihks}} \tag{11}$$

and

$$B_{ls}(\omega) = \frac{\Gamma_0}{\pi}\sum_{ihk}\frac{\left(\zeta_{hk}^2+\xi_{hk}^2\right)f(\varepsilon_{ihk})\mathrm{Re}[\eta_s(\varepsilon_{ihk})\langle\langle d_{\bar{s}}; d_{\bar{s}}^\dagger\rangle\rangle]}{\omega-\varepsilon_{lihks}}. \tag{12}$$

The impurity GF can be self-consistently calculated with the above formulism.

At low temperature, the magnetic susceptibility directly reflects the Kondo screening of a magnetic impurity in the hosts. The susceptibility is defined as $\chi_d = \frac{g\mu_B|n_{d\uparrow}-n_{d\downarrow}|}{\mathcal{H}}|_{\mathcal{H}\to 0}$, where μ_B denotes the Bohr magneton, g is the Landé factor, and $\mathcal{H}$ represents a weak magnetic field. And we take $\mu_B = g = 1$ in the present work. When the chemical potential lies at the Weyl nodes ($\mu = 0$), the magnetic susceptibility shows significant enhancement with the increase of coupling Γ_0 as shown in Fig. 4(a). This is attributed to the fact that the linear dispersion near the Weyl nodes leads to the anomalous broadening of the impurity level, see the inset of Fig. 4(a). The impurity level becomes more close to Weyl nodes after being renormalized by increasing the coupling Γ_0. The half-width of the broadened

impurity level narrows as the DOS of carriers decreases. In this case, the Kondo screening of the magnetic impurity is so weak that can be neglected due to the lack of DOSs around the Weyl nodes. By increasing the temperature, the suppression of susceptibility can be described by the Curie-Weiss law $\chi_d = c/(T + T_0)$, where c is a constant, and T_0 characterizes the localized magnetic states. By fitting the curves in Fig. 4(a), the coupling amplitude $\Gamma_0(= 1.0, 1.5, 1.75)$ corresponds to the parameters $c(= 0.45, 0.55, 0.66)$ and $T_0(= 0.1, 0.04, 0.025)$, respectively. It is noted that the Kondo screening is absent due to the pseudogapped DOSs at the nodes [41,49]. The magnetic susceptibility is enhanced by increasing the chirality imbalance $\delta\mu$ at low temperature, see Fig. 4(b). Here the chiral anomaly enhances the coupling between the magnetic impurity and conduction electrons, and hence the localized magnetic moment due to the anomalous broadening of the impurity level. In the inset of Fig. 4(b), we plot the temperature dependent local density of states (LDOS) of the magnetic impurity with $\delta\mu = 0.08$. The peak in the LDOS is enhanced by increasing the temperature T. This is the reason that the susceptibility is enhanced at the temperature $T < 0.01$, and then it is suppressed due to the thermal fluctuations for $T > 0.01$ as shown in Fig. 4(b).

The Kondo effect of magnetic impurity takes place by tuning the chemical potential away from the Weyl nodes. In this case, the magnetic susceptibility is determined by two factors: the enhancement of magnetic susceptibility due to anomalous broadening of impurity level near the Weyl nodes, see the inset of Fig. 4(a), and the suppression of the local moments by the Kondo screening. In Figs. 5(a) and 5(b) the low-temperature susceptibility displays typical Kondo screening behavior of the magnetic impurity in the absence of chiral anomaly as shown by the black lines $\delta\mu = 0$ [60,61]. The magnetic susceptibility is suppressed with the increasing of chirality imbalance $\delta\mu$. This is attributed to the chirality imbalance induced Kondo splitting in the LDOS of the impurity. As shown in the insets of Figs. 5(a) and 5(b), the subpeak of Kondo resonance at μ_- gets close to the impurity level, which enhances the broadening of the impurity levels. While the Kondo resonance peak at μ_+ is suppressed due to the increasing of $|\mu_+ - \varepsilon_d|$. Although the Kondo effect is taking place at low temperatures, the susceptibility is different from the conventional Kondo screening behaviors due to the chiral anomaly. The magnetic susceptibility is monotonously suppressed with T for the chemical potential above the nodes with $\mu_0 = 0.3$, as shown in Fig. 5(a). In this case, the Kondo screening has been suppressed due to the lack of DOS near the Weyl nodes even with the decreasing of $|\varepsilon_d - \mu_-|$. However, the Kondo screening is significantly enhanced for the chemical potential below the Weyl nodes ($\mu_0 = -0.2$), as shown in Fig. 5(b). This is due to the increasing of DOS of conduction electrons when μ_- gets close to the impurity level ε_d. In the presence of chiral anomaly, the opposite behaviors of the magnetic susceptibly for the chemical potential $\mu_0 > 0$ and $\mu_0 < 0$ originate from the particular band structure near the Weyl nodes.

The Kondo screening of a magnetic impurity originates from the coherent spin-flipping scattering (SFS) processes. Where an electron on the impurity level is replaced by a conduction electron with opposite spin through the empty or double occupied virtual states. In the bulk of Weyl SMs, the Kondo screening may contribute from both the internode and

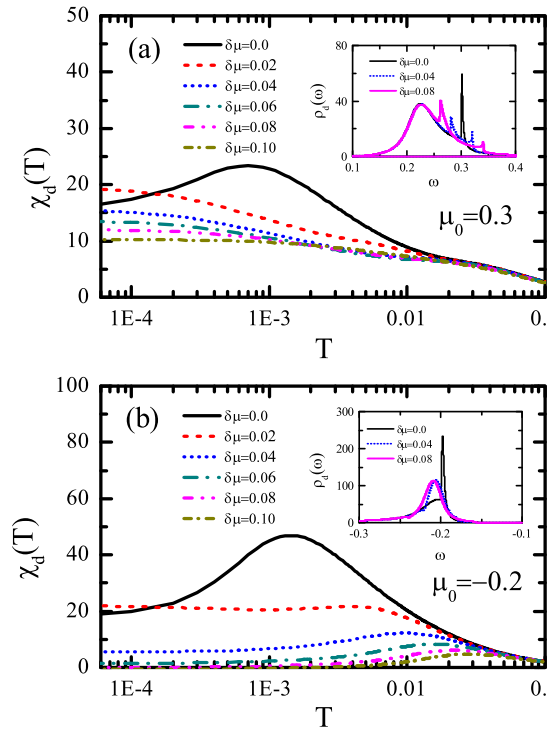

FIG. 5. The magnetic susceptibility of an impurity in Weyl SMs with finite DOSs at the Fermi level. (a) The chirality imbalance $\delta\mu$ dependent susceptibility for the chemical potential above the Weyl nodes with $\mu_0 = 0.3$, the coupling amplitude $\Gamma_0 = 0.5$, the impurity level $\varepsilon_d = 0.2$, and the Coulomb repulsion $U = 2.0$. (b) The susceptibility varying with the chirality imbalance $\delta\mu$ for the chemical potential posited below the Weyl nodes, and the parameters are $\mu_0 = -0.2$, $\Gamma_0 = 0.4$, $\varepsilon_d = -0.3$, $Q_z = 0.1$, and $U = 2.0$. The insets in (a) and (b) are the LDOS of the magnetic impurity with $\delta\mu = 0.0, 0.04, 0.08$.

the intranode spin-flipping scattering processes. In the absence of chirality anomaly ($\mu_+ = \mu_-$), the magnetic impurity is equally coupled with the Weyl nodes in the momentum space. There is no difference between the internode and intranode scattering processes because the Kondo screening is mainly determined by the conduction electrons near the Fermi levels. In the presence of chiral anomaly, however, the internode scattering would be suppressed due to the energy difference between Fermi levels of the nodes. In this case, the intranode SFS still contributes to the Kondo screening. There are two Kondo resonance peaks or antiresonance dip structures which appear at the chemical potentials $\omega = \mu_\pm$, as shown in the insets of Figs. 5(a) and 5(b). The antiresonance dips originate from the Fano interference between the Kondo resonance and the significant broadened impurity level [62].

In the experiment, the chiral anomaly in Weyl SMs has been introduced by the parallel magnetic and electric fields [19,20]. The Kondo resonance peaks at the chemical potentials $\mu_\pm = \mu_0 \pm \delta\mu$ would be split with four subpeaks or dips by the Zeeman interaction, as shown in Figs. 6(b) and 6(c). When the Zeeman interaction compensates the chirality imbalance $Ez = \delta\mu$, the magnetic impurity can be screened by the internode SFS processes as shown schematically in Fig. 6(a). The spin-down electron on the impurity level is replaced by a spin-up

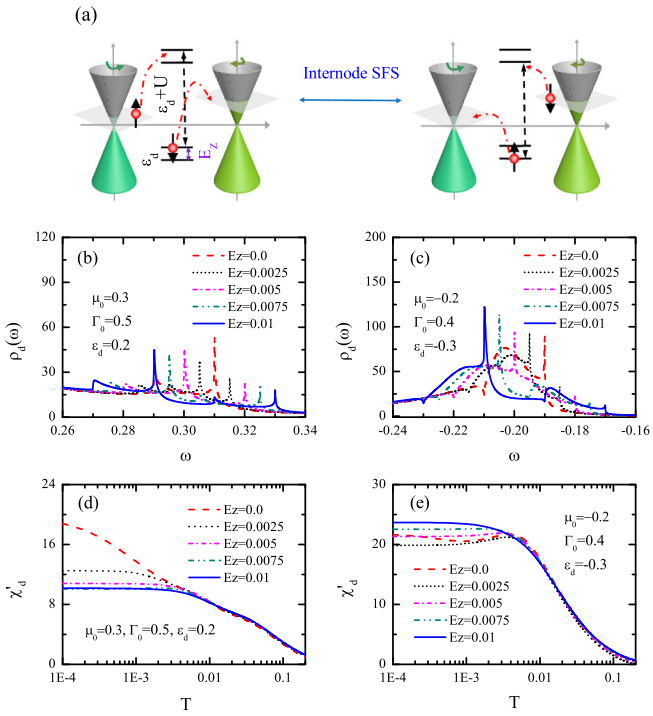

FIG. 6. (a) The schematic diagram of the Zeeman splitting induced coherent internode spin-flipping scattering (SFS) processes in the Weyl SMs with chiral anomaly. (b) The Zeeman splitting of the Kondo resonance in the local DOS with the parameters $\mu_0 = 0.3$, $\varepsilon_d = 0.2$, $\Gamma_0 = 0.5$, $Q_z = 0.1$, $U = 2$, $T = 0$, and $\delta\mu = 0.02$. The Zeeman interaction is arranged from $Ez = 0$ to $Ez = 0.01$. (c) The Zeeman splitting of Kondo resonance for the chemical potentials situated below the Weyl nodes with $\mu_0 = -0.2$, the impurity level $\varepsilon_d = -0.3$, and the coupling amplitude $\Gamma_0 = 0.4$. Other parameters are the same with that in (b). (e) and (f) The temperature dependent susceptibilities correspond to the chemical potential situated above and below the Weyl nodes in (b) and (c), respectively.

electron from the node with the chirality $h = -$, and the spin-down electron hops into the node with opposite chirality. Sequently the spin-up electron on the impurity is replaced by a spin-down electron on the node $h = +$. These coherent internode SFS processes lead to the Kondo resonance peaks reoccurring at the chemical potentials $\omega = \mu_\pm$ as shown in the blue solid lines in Figs. 6(b) and 6(c). In order to discuss the influence of Zeeman interaction on the localized magnetic states, we redefine the magnetic susceptibility $\chi_d^{'} = \frac{g\mu_B|n_{d\uparrow}-n_{d\downarrow}|}{\mathcal{H}_0+\mathcal{H}}|_{\mathcal{H}\to 0}$ with $\mathcal{H}_0 = E_z/(g\mu_B)$. For the chemical potential situated above the Weyl nodes ($\mu_0 = 0.3$), the Kondo screening has been suppressed by the chiral anomaly, see Fig. 5(a). In this case, the low-temperature susceptibility is suppressed due to the Zeeman interaction, as shown in Fig. 6(d). When the chemical potential is tuned below the Weyl nodes ($\mu_0 = -0.2$), the Kondo screening is significantly enhanced due to chiral anomaly. At low temperatures, the magnetic susceptibility is enhanced by the Zeeman interaction, as shown in Fig. 6(e). The is due to the Kondo screening of magnetic impurity suppressed by the Zeeman splitting. The signature of Kondo screening even extends to $E_z = 0.02$, see the blue solid line in Fig. 6(e). Therefore, the chiral anomaly enhanced Kondo screening can be observed when the Zeeman splitting is not large enough.

V. CONCLUSION

In this work we have studied the localized magnetic states and the Kondo screening of a magnetic impurity in the bulk of Weyl SMs. The anomalous broadening of the impurity level leads to a nonvanishing magnetic moment in wide range of parameters. The phase boundary between the magnetic and nonmagnetic regions exhibits a particle-hole asymmetric due to the linear dispersion near the Weyl nodes. When the chemical potential lies at the nodes $\mu_0 = 0$, the Kondo effect is absent due to the vanishing of DOSs. The susceptibility is significantly enhanced at low temperatures due the chirality imbalance. The Kondo screening takes place at finite chemical potential $\mu_0 \neq 0$. The magnetic susceptibility is determined by both the Kondo screening and the broadening of the impurity level near the Weyl nodes. When the chemical potential is tuned above the Weyl nodes $\mu_0 > 0$, the Kondo screening is suppressed by the chiral anomaly. Oppositely, the Kondo screening is significantly enhanced by the chirality imbalance for $\mu_0 < 0$. Due to the Kondo screening of the magnetic impurity, the chiral anomaly in Weyl SMs can be detected through the measurement of low-temperature susceptibility.

ACKNOWLEDGMENTS

We acknowledge useful discussion with Rui Chen, Hua Chen, Wei Chen, and Hao-Ran Chang. This work is supported by the National Key Research and Development Program of China (No. 2016YFA0300300), and NSFC (No. 11604138, No. 11674151, No. 11604166, No. 11704106, No. 11547110, No. 11674139), PCSIRT (No. IRT-16R35) of China, the Scientific Research Project of Education Department of Hubei Province (No. Q20171005).

APPENDIX

In the Appendix we outline the treatment of the Green's function $\langle\langle d_s n_{d\bar{s}}; d_s^\dagger\rangle\rangle$ with the Lacroix's approximation scheme. The EOM of the higher-order GF reads

$$\begin{aligned}(\omega - \varepsilon_{ds} - U)\langle\langle d_s n_{d\bar{s}}; d_s^\dagger\rangle\rangle &= \langle n_{d\bar{s}}\rangle + \sum_{ih\mathbf{k}} V_{ihks}^*\langle\langle \alpha_{ih\mathbf{k}} n_{d\bar{s}}; d_s^\dagger\rangle\rangle \\ &+ \sum_{ih\mathbf{k}} V_{ihks}\langle\langle \alpha_{ih\mathbf{k}}^\dagger d_{\bar{s}} d_s; d_s^\dagger\rangle\rangle \\ &- \sum_{ih\mathbf{k}} V_{ihks}^*\langle\langle d_{\bar{s}}^\dagger \alpha_{ih\mathbf{k}} d_s; d_s^\dagger\rangle\rangle, \end{aligned} \tag{A1}$$

which generates some high-order GFs, such as $\langle\langle \alpha_{ih\mathbf{k}} n_{d\bar{s}}; d_s^\dagger\rangle\rangle$, $\langle\langle \alpha_{ih\mathbf{k}}^\dagger d_{\bar{s}} d_s; d_s^\dagger\rangle\rangle$, and $\langle\langle d_{\bar{s}}^\dagger \alpha_{ih\mathbf{k}} d_s; d_s^\dagger\rangle\rangle$. From Eq. (7), One can gain the EOM of these GFs as follows:

$$\begin{aligned}(\omega - \varepsilon_{ihk})\langle\langle \alpha_{ih\mathbf{k}} n_{d\bar{s}}; d_s^\dagger\rangle\rangle \\ \approx V_{ihks}\langle\langle d_s n_{d\bar{s}}; d_s^\dagger\rangle\rangle\end{aligned}$$

$$+\sum_{i'h'\mathbf{k}'} V_{i'h'k's}\langle\langle\alpha^{\dagger}_{i'h'\mathbf{k}'}d_{\bar{s}}\alpha_{ih\mathbf{k}};d^{\dagger}_{s}\rangle\rangle$$
$$-\sum_{i'h'\mathbf{k}'} V^{*}_{i'h'k's}\langle\langle d^{\dagger}_{\bar{s}}\alpha_{i'h'\mathbf{k}'}\alpha_{ih\mathbf{k}};d^{\dagger}_{s}\rangle\rangle, \quad \text{(A2)}$$

$$(\omega+\varepsilon_{ihk}-\varepsilon_{ds}-\varepsilon_{d\bar{s}}-U)\langle\langle\alpha^{\dagger}_{ih\mathbf{k}}d_{\bar{s}}d_{s};d^{\dagger}_{s}\rangle\rangle$$
$$\approx\langle\alpha^{\dagger}_{ih\mathbf{k}}d_{\bar{s}}\rangle+V^{*}_{ihks}\langle\langle d_{s}n_{\bar{s}};d^{\dagger}_{s}\rangle\rangle$$
$$-\sum_{i'h'\mathbf{k}'} V_{i'h'k's}\langle\langle\alpha^{\dagger}_{ih\mathbf{k}}\alpha_{i'h'\mathbf{k}'}d_{s};d^{\dagger}_{s}\rangle\rangle$$
$$+\sum_{i'h'\mathbf{k}'} V^{*}_{i'h'k's}\langle\langle\alpha^{\dagger}_{ih\mathbf{k}}d_{\bar{s}}\alpha_{i'h'\mathbf{k}'};d^{\dagger}_{s}\rangle\rangle, \quad \text{(A3)}$$

and

$$(\omega-\varepsilon_{ihk}+\varepsilon_{d\bar{s}}-\varepsilon_{ds})\langle\langle d^{\dagger}_{\bar{s}}\alpha_{ih\mathbf{k}}d_{s};d^{\dagger}_{s}\rangle\rangle$$
$$\approx\langle d^{\dagger}_{\bar{s}}\alpha_{ih\mathbf{k}}\rangle-V_{ihks}\langle\langle d_{s}n_{\bar{s}};d^{\dagger}_{s}\rangle\rangle$$
$$+\sum_{i'h'\mathbf{k}'} V_{i'h'k's}\langle\langle\alpha^{\dagger}_{i'h'\mathbf{k}'}\alpha_{ih\mathbf{k}}d_{s};d^{\dagger}_{s}\rangle\rangle$$
$$+\sum_{i'h'\mathbf{k}'} V^{*}_{i'h'k's}\langle\langle d^{\dagger}_{\bar{s}}\alpha_{ih\mathbf{k}}\alpha_{i'h'\mathbf{k}'};d^{\dagger}_{s}\rangle\rangle. \quad \text{(A4)}$$

In these equations, the Lacroix's treatment can be reached by taking the approximation, such as $\langle\langle\alpha^{\dagger}_{i'h'\mathbf{k}'}d_{\bar{s}}\alpha_{ih\mathbf{k}};d^{\dagger}_{s}\rangle\rangle\approx\langle\alpha^{\dagger}_{i'h'\mathbf{k}'}d_{\bar{s}}\rangle\langle\langle\alpha_{ih\mathbf{k}};d^{\dagger}_{s}\rangle\rangle$ and $\langle\langle\alpha^{\dagger}_{ih\mathbf{k}}\alpha_{i'h'\mathbf{k}'}d_{s};d^{\dagger}_{s}\rangle\rangle\approx\langle\alpha^{\dagger}_{ih\mathbf{k}}\alpha_{i'h'\mathbf{k}'}\rangle\langle\langle d_{s};d^{\dagger}_{s}\rangle\rangle$. By substituting Eqs. (A2)–(A4) into Eq. (A1), one can obtain

$$\langle\langle d_{s}n_{d\bar{s}};d^{\dagger}_{s}\rangle\rangle=\frac{\langle n_{d\bar{s}}\rangle+Q_{s}(\omega)-\Phi_{s}(\omega)\langle\langle d_{s};d^{\dagger}_{s}\rangle\rangle}{\omega-\varepsilon_{ds}-U-\Xi^{0}_{s}(\omega)-\Xi^{1}_{s}(\omega)-\Xi^{2}_{s}(\omega)}, \quad \text{(A5)}$$

where $\eta_{s}(\omega)=1+\frac{\Xi^{0}_{s}(\omega)}{\omega-\varepsilon_{d\bar{s}}-\Xi^{0}_{s}(\omega)}$, $\Xi^{1(2)}_{s}(\omega)=\sum_{ihk}\frac{|V_{sihk}|^{2}}{\omega-\varepsilon_{1(2)ihks}}$, $\varepsilon_{1ihks}=-\varepsilon_{ihk}+\varepsilon_{d\bar{s}}+\varepsilon_{ds}+U$, and $\varepsilon_{2ihks}=\varepsilon_{ihk}-\varepsilon_{d\bar{s}}+\varepsilon_{ds}$.

Other notations are $\Phi_{s}(\omega)=\Omega_{s}(\omega)+Q_{s}(\omega)\Xi^{0}_{s}(\omega)\eta_{s}(\omega)$, $\Omega_{s}(\omega)=A_{1s}(\omega)+A_{2s}(\omega)$ and $Q_{s}(\omega)=B_{1s}(\omega)-B_{2s}(\omega)$ with

$$A_{1s}(\omega)=\sum_{ih\mathbf{k}}\sum_{i'h'\mathbf{k}'}\frac{V^{*}_{sihk}V_{si'h'k'}\langle\alpha^{\dagger}_{i'h'\mathbf{k}'}\alpha_{ih\mathbf{k}}\rangle}{\omega-\varepsilon_{1ihks}}, \quad \text{(A6)}$$

$$A_{2s}(\omega)=\sum_{ih\mathbf{k}}\sum_{i'h'\mathbf{k}'}\frac{V_{sihk}V^{*}_{si'h'k'}\langle\alpha^{\dagger}_{ih\mathbf{k}}\alpha_{i'h'\mathbf{k}'}\rangle}{\omega-\varepsilon_{2ihks}}, \quad \text{(A7)}$$

$$B_{1s}=\sum_{ih\mathbf{k}}\frac{V^{*}_{sihk}\langle d^{\dagger}_{\bar{s}}\alpha_{ih\mathbf{k}}\rangle}{\omega-\varepsilon_{1ihks}}, \quad \text{(A8)}$$

$$B_{2s}=\sum_{ih\mathbf{k}}\frac{V_{sihk}\langle\alpha^{\dagger}_{ih\mathbf{k}}d_{\bar{s}}\rangle}{\omega-\varepsilon_{2ihks}}. \quad \text{(A9)}$$

From the spectral theorem, one can obtain

$$\Xi^{1(2)}_{s}(\omega)=\frac{\Gamma_{0}}{\pi}\sum_{k}\frac{\zeta^{2}_{hk}+\xi^{2}_{hk}}{\omega-\varepsilon_{1(2)ihks}}, \quad \text{(A10)}$$

$$A_{1(2)s}(\omega)\approx\frac{\Gamma_{0}}{\pi}\sum_{ihk}\frac{(\zeta^{2}_{hk}+\xi^{2}_{hk})f(\varepsilon_{ihk})}{\omega-\varepsilon_{1(2)ihks}}, \quad \text{(A11)}$$

and

$$B_{1(2)s}(\omega)\approx\frac{\Gamma_{0}}{\pi}\sum_{ihk}\frac{(\zeta^{2}_{hk}+\xi^{2}_{hk})f(\varepsilon_{ihk})\mathrm{Re}[\eta_{s}(\varepsilon_{ihk})\langle\langle d_{\bar{s}};d^{\dagger}_{\bar{s}}\rangle\rangle]}{\omega-\varepsilon_{1(2)ihks}}. \quad \text{(A12)}$$

By substituting Eq. (A5) into Eq. (8) in the main text, one can gain the impurity GF

$$\langle\langle d_{s};d^{\dagger}_{s}\rangle\rangle=\frac{1+U\frac{\langle n_{d\bar{s}}\rangle+Q_{s}(\omega)}{\omega-\varepsilon_{ds}-U-\Xi_{s}(\omega)}}{\omega-\varepsilon_{ds}-\Xi^{0}_{s}(\omega)\eta_{s}(\omega)+U\frac{\Omega_{s}(\omega)+Q_{s}(\omega)\Xi^{0}_{s}(\omega)\eta_{s}(\omega)}{\omega-\varepsilon_{ds}-U-\Xi_{s}(\omega)}}, \quad \text{(A13)}$$

with $\Xi_{s}(\omega)=\Xi^{0}_{s}(\omega)+\Xi^{1}_{s}(\omega)+\Xi^{2}_{s}(\omega)$.

[1] C. L. Kane and E. J. Mele, Phys. Rev. Lett. **95**, 146802 (2005); **95**, 226801 (2005).
[2] X. L. Qi and S. C. Zhang, Rev. Mod. Phys. **83**, 1057 (2011).
[3] N. Read and D. Green, Phys. Rev. B **61**, 10267 (2000).
[4] L. Fu and C. L. Kane, Phys. Rev. Lett. **100**, 096407 (2008).
[5] J. Alicea, Rep. Prog. Phys. **75**, 076501 (2012).
[6] B. A. Bernevig, T. L. Hughes, and S. C. Zhang, Science **314**, 1757 (2006).
[7] L. Fu, C. L. Kane, and E. J. Mele, Phys. Rev. Lett. **98**, 106803 (2007).
[8] M. Z. Hasan and C. L. Kane, Rev. Mod. Phys. **82**, 3045 (2010).
[9] Z. K. Liu, B. Zhou, Y. Zhang, Z. Wang, H. Weng, D. Prabhakaran, S.-K. Mo, Z. Shen, Z. Fang, X. D. Z. Hussain, and Y. L. Chen, Science **343**, 864 (2014).
[10] Z. K. Liu, J. Jiang, B. Zhou, Z. J. Wang, Y. Zhang, H. M. Weng, D. Prabhakaran, S.-K. Mo, H. Peng, P. Dudin, T. Kim, M. Hoesch, Z. Fang, X. Dai, Z. X. Shen, D. L. Feng, Z. Hussain, and Y. L. Chen, Nat. Mater. **13**, 677 (2014).
[11] L. P. He, X. C. Hong, J. K. Dong, J. Pan, Z. Zhang, J. Zhang, and S. Y. Li, Phys. Rev. Lett. **113**, 246402 (2014).
[12] S. Borisenko, Q. Gibson, D. Evtushinsky, V. Zabolotnyy, B. Buchner, and R. J. Cava, Phys. Rev. Lett. **113**, 027603 (2014).
[13] M. Neupane, S.-Y. Xu, R. Sankar, N. Alidoust, G. Bian, C. Liu, I. Belopolski, T.-R. Chang, H.-T. Jeng, H. Lin *et al.*, Nat. Commun. **5**, 3786 (2014).
[14] X. Wan, A. M. Turner, A. Vishwanath, and S. Y. Savrasov, Phys. Rev. B **83**, 205101 (2011).
[15] L. X. Yang, Z. K. Liu, Y. Sun, H. Peng, H. F. Yang, T. Zhang, B. Zhou, Y. Zhang, Y. F. Guo, M. Rahn, D. Prabhakaran, Z. Hussain, S.-K. Mo, C. Felser, B. Yan, and Y. L. Chen, Nat. Phys. **11**, 728 (2015).
[16] B. Q. Lv, H. M. Weng, B. B. Fu, X. P. Wang, H. Miao, J. Ma, P. Richard, X. C. Huang, L. X. Zhao, G. F. Chen, Z. Fang, X. Dai, T. Qian, and H. Ding, Phys. Rev. X **5**, 031013 (2015).
[17] S.-Y. Xu *et al.*, Science, **349**, 613 (2015).
[18] Y. Li, Z. Wang, P. Li, X. Yang, Z. Shen, F. Sheng, X. Li, Y. Lu, Y. Zheng, and Z.-A. Xu, Front. Phys. **12**, 127205 (2017).
[19] A. A. Burkov, Phys. Rev. Lett. **113**, 247203 (2014).
[20] C. L. Zhang *et al.*, Nat. Commun. **7**, 10735 (2016).
[21] H. B. Nielsen and M. Ninomiya, Phys. Lett. B **130**, 389 (1983).
[22] D. T. Son and B. Z. Spivak, Phys. Rev. B **88**, 104412 (2013).

[23] X. Huang, L. Zhao, Y. Long, P. Wang, D. Chen, Z. Yang, H. Liang, M. Xue, H. Weng, Z. Fang, X. Dai, and G. Chen, Phys. Rev. X **5**, 031023 (2015).
[24] X. Yang, Y. Li, Z. Wang, Y. Zhen, and Z.-A. Xu, arXiv:1506.02283.
[25] C.-Z. Li, L.-X. Wang, H. Liu, J. Wang, Z.-M. Liao, and D.-P. Yu, Nat. Commun. **6**, 10137 (2015).
[26] S. A. Parameswaran, T. Grover, D. A. Abanin, D. A. Pesin, and A. Vishwanath, Phys. Rev. X **4**, 031035 (2014).
[27] P. E. C. Ashby and J. P. Carbotte, Phys. Rev. B **89**, 245121 (2014).
[28] P. Goswami, G. Sharma, and S. Tewari, Phys. Rev. B **92**, 161110(R) (2015).
[29] P. Hosur and X.-L. Qi, Phys. Rev. B **91**, 081106(R) (2015).
[30] J. Zhou and H.-R. Chang, Phys. Rev. B **97**, 075202 (2018).
[31] J. Zhou, H.-R. Chang, and D. Xiao, Phys. Rev. B **91**, 035114 (2015).
[32] J. Kondo, Prog. Theor. Phys. **32**, 37 (1964).
[33] A. C. Hewson, *The Kondo Problem to Heavy Fermions* (Cambridge University Press, Cambridge, 1993).
[34] S. M. Cronenwett, T. H. Oosterkamp, and L. P. Kouwenhoven, Science **281**, 540 (1998).
[35] V. Madhavan, W. Chen, T. Jamneala, M. F. Crommie, and N. S. Wingreen, Science **280**, 567 (1998).
[36] W. G. van der Wiel, S. De Franceschi, T. Fujisawa, J. M. Elzerman, S. Tarucha, and L. P. Louwenhoven, Science **289**, 2105 (2000).
[37] H. Jeong, A. M. Chang, and M. R. Melloch, Science **293**, 2221 (2001).
[38] A. V. Balatsky, I. Vekhter, and J.-X. Zhu, Rev. Mod. Phys. **78**, 373 (2006).
[39] J.-H. Chen, L. Li, W. G. Cullen, E. D. Williams, and M. S. Fuhrer, Nat. Phys. **7**, 535 (2011).
[40] J.-H. Sun, D.-H. Xu, F.-C. Zhang, and Y. Zhou, Phys. Rev. B **92**, 195124 (2015).
[41] A. K. Mitchell and L. Fritz, Phys. Rev. B **92**, 121109(R) (2015).
[42] A. Principi, G. Vignale, and E. Rossi, Phys. Rev. B **92**, 041107(R) (2015).
[43] J.-H. Sun, L.-J. Wang, X.-T. Hu, L. Li, and D.-H. Xu, Phys. Rev. B **97**, 035130 (2018).
[44] D. Ma, H. Chen, H.-W. Liu, and X. C. Xie, Phys. Rev. B **97**, 045148 (2018).
[45] H.-R. Chang, J. Zhou, S.-X. Wang, W.-Y. Shan, and D. Xiao, Phys. Rev. B **92**, 241103(R) (2015).
[46] B. Uchoa, V. N. Kotov, N. M. R. Peres, and A. H. C. Neto, Phys. Rev. Lett. **101**, 026805 (2008); **101**, 039903(E) (2008).
[47] M. Mashkoori, I. Mahyaeh, and S. A. Jafari, J. Phys.: Conf. Ser. **603**, 012015 (2015).
[48] Y. Mohammadi and R. Moradian, Solid State Commun. **178**, 37 (2014).
[49] P. S. Cornaglia, G. Usaj, and C. A. Balseiro, Phys. Rev. Lett. **102**, 046801 (2009).
[50] S.-P. Chao and V. Aji, Phys. Rev. B **83**, 165449 (2011).
[51] K. Sengupta and G. Baskaran, Phys. Rev. B **77**, 045417 (2008).
[52] M. Vojta, L. Fritz, and R. Bulla, Europhys. Lett. **90**, 27006 (2010).
[53] P. W. Anderson, Phys. Rev. **124**, 41 (1961).
[54] D. N. Zubarev, Usp. Fiz. Nauk. **71**, 71 (1960); Sov. Phys. Usp. **3**, 320 (1960).
[55] A.-P. Jauho, N. S. Wingreen, and Y. Meir, Phys. Rev. B **50**, 5528 (1994).
[56] R. Świrkowicz, J. Barnaś, and M. Wilczyński, Phys. Rev. B **68**, 195318 (2003).
[57] L. Li, Y.-Y. Ni, Y. Zhong, T.-F. Fang, and H.-G. Luo, New J. Phys. **15**, 053018 (2013).
[58] C. Lacroix, J. Phys. F **11**, 2389 (1981).
[59] H.-G. Luo, Z.-J. Ying, and S.-J. Wang, Phys. Rev. B **59**, 9710 (1999).
[60] L. Merker, A. Weichselbaum, and T. A. Costi, Phys. Rev. B **86**, 075153 (2012).
[61] T.-F. Fang, N.-H. Tong, Z. Cao, Q.-F. Sun, and H.-G. Luo, Phys. Rev. B **92**, 155129 (2015).
[62] H. G. Luo, T. Xiang, X. Q. Wang, Z. B. Su, and L. Yu, Phys. Rev. Lett. **92**, 256602 (2004).